A self-consistent approach to the analysis of thermionic devices

Amir H. Khoshaman and Alireza Nojeh

Citation: Journal of Applied Physics **119**, 044902 (2016); doi: 10.1063/1.4940673
View online: http://dx.doi.org/10.1063/1.4940673
View Table of Contents: http://scitation.aip.org/content/aip/journal/jap/119/4?ver=pdfcov
Published by the AIP Publishing

JOURNAL OF APPLIED PHYSICS **119**, 044902 (2016)

A self-consistent approach to the analysis of thermionic devices

Amir H. Khoshaman[a)] and Alireza Nojeh[a)]
Department of Electrical and Computer Engineering, University of British Columbia, Vancouver, British Columbia V6T 1Z4, Canada

(Received 16 September 2015; accepted 9 January 2016; published online 27 January 2016)

Research in thermionics has been reinvigorated recently by the advent of nanotechnology and nanomaterials. Thermionic energy convertors are commonly modelled using the Poisson-Vlasov system of equations under various limitations and approximations. With the ever-growing demands of emergent thermionic devices, more comprehensive approaches are needed in order to be able to treat a broader range of device configurations and operational parameters. Here, we propose a self-consistent approach that, by iterating between the Poisson and Vlasov equations, does not rely on the existence of an analytical solution to the latter. Specifically, we present a particle-tracing implementation of this method for solving the system numerically in an efficient manner. In the case where an analytical solution does exist, we present an asymptotic expansion of the ill-behaving functions that arise; this approach improves the effectiveness of the method in the deep space-charge mode. We also demonstrate the applicability of this approach in the presence of back-emission. © *2016 AIP Publishing LLC*. [http://dx.doi.org/10.1063/1.4940673]

INTRODUCTION

Thermionic energy convertors (TECs) offer promising features such as an exponential dependence of current density on temperature, high power density and current density, significant simplicity compared to mechanical heat engines, and, in the case of solar energy conversion, the ability to harness a broad spectral range of the incident light. These properties make TECs highly appealing for inexpensive and clean energy applications. Typically, a TEC comprises two electrodes (emitter and collector) isolated by a vacuum gap (Fig. 1(a)). Electrons in the high-energy Fermi tail in the hotter electrode (emitter) have sufficient kinetic energy to circumvent the energy barrier; some of them are emitted into the vacuum gap, traverse the inter-electrode distance, and are condensed on the collector. The electrons subsequently find their way back to the emitter through an external load. The difference between the electrochemical potentials of the electrodes determines the voltage generated across the load.

TECs have been studied for a century for direct conversion of heat to electricity. However, a new wave of interest has recently emerged due to the advances in micro- and nanofabrication and the properties of nanomaterials, which have opened up new opportunities for addressing the challenges of these devices.[1–6] A survey of some of the advances in thermionic conversion enabled by nanotechnology is given in Ref. 7. (Here, we note that, as pointed out in Ref. 5, given that these devices are concerned with electron emission and not ion emission, they may more appropriately be called thermoelectronic energy convertors, for which again the same acronym, TEC, can be used.)

A method commonly used for the analysis of TECs was developed several decades ago by Langmuir, Hatsopoulos, and Gyftopoulos.[8,9] It involves solving the Poisson-Vlasov system of equations in the space-charge limited (SCL) regime, assuming the electrons in the inter-electrode space follow the dynamics of a steady-state collisionless gas (albeit having Coulomb interactions in an average manner) with a hemi-Maxwellian (HM) velocity distribution;[8,10] this approach results in an analytical solution in the form of an integral, which can then be calculated numerically.

In this method, the solutions only exist when the motive reaches a maximum in the inter-electrode distance. It is because analytical solutions, in a closed form, arise when the boundary conditions are enforced such that the derivative of the motive is zero at one point in the inter-electrode region. This condition significantly narrows down the applicability of the analytical solution in the modes of operation that are not space-charge limited. This effect is most palpable at the boundaries between the retarding mode and the space-charge mode, where the highest errors can occur if a combination of precise numerical integration and an iterative strategy are not employed.[11]

This method also has a limited range of applicability in the presence of strong space charge and suffers from high splicing errors due to employment of different equations for different regimes of operation. These limitations were overcome in our earlier works by solving the equations for a wider range of parameters and following a more robust algorithm.[11–13]

Smith *et al.*[4,14] developed the theory of TECs with a negative electron affinity (NEA) emitter using an approach similar to that of Langmuir and Hatsopoulos, and proposed a method to calculate the limits of the space-charge regime. Smith also proposed that the space-charge effect can be mitigated in the case of a TEC incorporating an NEA material as the anode.[16] Lee *et al.* have modeled the behavior of TECs with very small gaps where near-field heat transfer becomes important and have observed that the optimum gap roughly corresponds to the characteristic wavelength of the emitter's thermal radiation.[17]

[a)]Authors to whom correspondence should be addressed. Electronic addresses: akhosham@ece.ubc.ca and anojeh@ece.ubc.ca

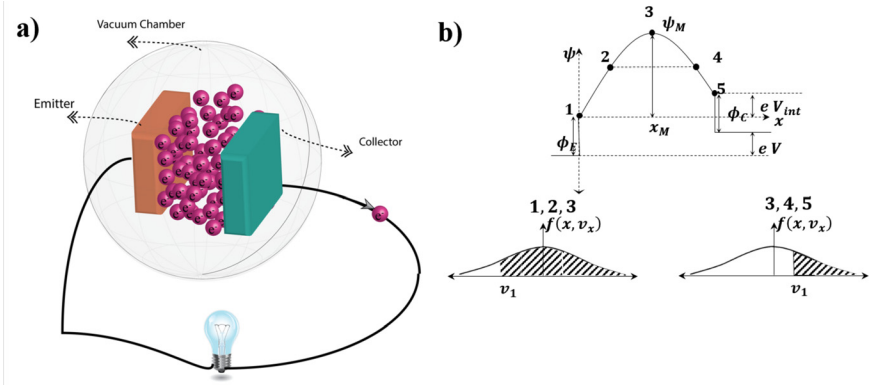

FIG. 1. (a) Schematic diagram of a TEC. The device comprises a hot emitter and a collector, separated through a vacuum gap. The electrodes are connected externally through a load (represented by a bulb). (b) The motive diagram and the corresponding velocity distributions in the space-charge limited mode of operation.

Another approach was adopted by Meir *et al.*,[5,15] which involves solving the differential equation that is obtained by replacing the analytical solution to the Vlasov equation, inside the Poisson equation, and employing a non-linear self-consistent solver. This method can treat all regimes of operation and overcome the splicing errors; however, the solution is limited to the cases where an analytical solution to the Vlasov equation exists, e.g., when the TEC comprises two infinitely large and uniformly heated flat electrodes.

Here, we develop a strategy that consists of iterating between the two equations and can be used even for cases where the Vlasov equation does not have an analytical solution. As a way of efficiently obtaining a numerical solution, we present a particle tracing approach to calculate the electron density. Although we present the 1-dimensional case, this strategy can be expanded to include higher dimensions where an analytical solution to the Vlasov equation does not exist. This is an important issue, since in the absence of an analytical solution, the Vlasov equation lives in the 6-dimensional phase space, and finding a numerical solution to it can be extremely challenging and time-consuming. Our approach can also incorporate the analytical solution of the Vlasov equation; the applicability of the model in this case is significantly improved by employing an asymptotic expansion to calculate the ill-behaving functions involved in the solution of the Vlasov equation.

Dugan[19] employed Langmuir's theory of space charge in the presence of back-emission using a method similar to that of Hatsopoulos, i.e., starting with a current density and calculating the voltage that corresponds to this current. He developed an iterative approach, since the total current density depends on the unknown in the problem, i.e., the applied voltage. This approach naturally faces some of the challenges associated with Hatsopoulos' method, described above. It is indispensable to reliably include the presence of back-emission in the analysis of the emergent thermionic devices; by employing nanotechnology, ever smaller inter-electrode distances are achievable, which could lead to a higher temperature of the collector. In this paper, after describing the model, we develop the physics of the TEC in the presence of back-emission and present the output current-voltage characteristics.

The model presented here can be used to evaluate the output characteristics of TECs for a wide range of parameters, unless quantum tunneling (occurring at nanoscale inter-electrode distances) or relativistic effects (occurring at exceedingly high biases that are not relevant in thermionic convertors) are prevalent. We intentionally emphasize cases where the space charge effect is prominent, in order to demonstrate the applicability of the approach, and these situations naturally lead to low energy conversion efficiencies; however, the model is equally applicable to low-space-charge scenarios. The calculation of the conversion efficiency would involve, in addition to the electron transport characteristics obtained using the proposed approach, other considerations such as the heating mechanism of the emitter and power delivery to the external load, with the relevant parameters such as thermal conductivity, resistivity, and emissivity. Overall device modeling for the evaluation of efficiency has been discussed in previous works.[5,8,18]

THEORY AND MODEL

The thermionic emission current from the electrodes is calculated from the Richrdson-Dushman equation, $J_{sat} = A\,T^2 \exp\left(-\phi/k_B T\right)$, where J_{sat} is the saturation current density, T represents the temperature of either the emitter or the collector, k_B is the Boltzmann constant, ϕ is the workfunction, and $A = 1.202 \times 10^6\,\mathrm{A\,m^{-2}\,K^{-2}}$ is the Richardson-Dushman constant.[20] (Throughout the paper, we will use subscripts E and C to refer to the parameters of the emitter and collector, respectively, such as temperature and workfunction.) It is assumed that electrons originate from the emitter or the collector and are fully absorbed once they arrive at the opposite electrode. In the next section (Self-consistent solution in the absence of back-emission), we develop the model in the absence of back-emission and show that the results are in agreement with our improved-and-extended-Langmuir (IEL) solution reported earlier.[11] In a subsequent section (Self-consistent solution in the presence of back-emission), we use this model to analyze a TEC with substantial back-emission from its collector.

Self-consistent solution in the absence of back-emission

In a 1-D case and in the absence of magnetic fields, the steady-state collisionless Vlasov equation can be written as[21] $v_x \frac{\partial f(x,v_x)}{\partial x} - \frac{1}{m}\frac{d\psi(x)}{dx}\frac{\partial f(x,v_x)}{\partial v_x} = 0$, where x denotes the direction normal to the emitter's surface, $\psi(x)$ represents electron motive (in this case, electric potential energy), v_x is the

velocity of the electron along the direction of propagation, and $f(x, v_x)$ is the velocity distribution function.[22] The general solution to this equation can be written as the sum of functions of the form $a_i \exp\{-b_i(\psi + \frac{1}{2}m v^2)\}$, where v is the magnitude of the velocity vector (speed) of the electrons.[9] Langmuir[9] obtained the constants a_i and b_i by assuming that the electron velocity distribution adopts an HM form at the point of the maximum motive (x_M, ψ_M), namely, $f(x_M, v) = 2\,n(x_M)\left(\frac{m}{2\pi k_B T_E}\right)^{\frac{3}{2}} \exp\left(-\frac{mv^2}{2k_B T_E}\right) \times \Theta(v_x)$, where Θ represents the unit step function, and $n(x_M)$ is the electron density at $x = x_M$ (point 3 in Fig. 1(b)). The motivation behind this assumption is that electrons originate from one electrode (emitter), and therefore those with kinetic energies lower than ψ_M cannot surmount the maximum motive.[10] In the next section (Self-consistent solution in the presence of back-emission), we will provide arguments on the validity of this assumption in the case of the emergent TECs and also in the presence of back-emission.

The maximum motive, ψ_M, coincides with the points just outside the emitter or collector at the start of the flowchart in Fig. 2, in positive and negative applied voltages, respectively. However, the maximum motive can move inside the inter-electrode region in subsequent iterations. In that case, the device is operating in the SCL mode. If the maximum motive coincides with the points just outside the emitter or collector at the end of the loop, the device is operating in the saturation or retarding modes, respectively. As we will show, our strategy can be used in these modes as well.

The velocity distribution function, $f(x, v)$, can be calculated by considering the ranges of applicable velocities along different points in the inter-electrode region. Assuming that the emitter is positioned at $x = 0$ and the collector at $x = d$, the electrons lying on the left side of x_M (points 1–3 in Fig. 1(b)) can move bidirectionally, whereas electrons to the right of x_M (points 3–5 in Fig. 1(b)) naturally move only to the right. This behavior is again due to the fact that electrons originate from the emitter, and the ones that possess sufficient kinetic energy to overcome the ψ_M barrier, only move to the right at $x > x_M$. Therefore, the minimum velocity, $v_{x,min}$, is negative for $x < x_M$ and equal to $-v_{x,min} = -\left(2\frac{\psi_M - \psi(x)}{m}\right)^{\frac{1}{2}}$, corresponding to electrons that had a kinetic energy to barely make it to the peak, but not enough to overcome the barrier. By the same token, the minimum velocity, $v_{x,min}$, is positive for $x > x_M$ (since electrons only move to the right) and equal to $v_{x,min} = \left(2\frac{\psi_M - \psi(x)}{m}\right)^{\frac{1}{2}}$. Therefore, the velocity distribution function, $f(x, v_x)$, can be formulated as

$$f(x,v) = 2\,n(x_M)\left(\frac{m}{2\pi k_B T_E}\right)^{\frac{3}{2}} \exp\left(\frac{\psi_M - \psi(x)}{k_B T_E} - \frac{mv^2}{2k_B T_E}\right) \times \Theta\left(v_x \pm (v_x)_{min}\right), \tag{1}$$

for $x \le x_M$ (+ sign) and $x > x_M$ (− sign).[10]

The electron density, $n(x)$, is calculated by integration of the velocity distribution function as $n(x) = \int_{-\infty}^{\infty}\int_{-\infty}^{\infty}\int_{-\infty}^{\infty} f(x,v)\,dv_x\,dv_y\,dv_z$, resulting in

$$n(x) = n(x_M)\exp(\gamma_E)\begin{cases} 1 - \mathrm{erf}(\gamma_E{}^{1/2}), & x > x_M \\ 1 + \mathrm{erf}(\gamma_E{}^{1/2}), & x \le x_M, \end{cases} \tag{2}$$

where γ_E is the dimensionless motive for the electrons originating from the emitter defined as $(\psi_M - \psi(x))/k_B T_E$, and erf is the error function.[10]

Equation (2) is subsequently substituted into Poisson's equation to yield

$$\frac{d^2\psi(x)}{dx^2} = -\frac{e^2}{\epsilon_0} n(x_M)\exp(\gamma_E)\begin{cases} 1 - \mathrm{erf}(\gamma_E{}^{1/2}), & x > x_M \\ 1 + \mathrm{erf}(\gamma_E{}^{1/2}), & x \le x_M, \end{cases} \tag{3}$$

subject to the boundary conditions, $\psi(0) = 0$ and $\psi(d) = eV$, where e is the electron's charge (negative value), ϵ_0 is the permittivity of vacuum, and V is the voltage difference between

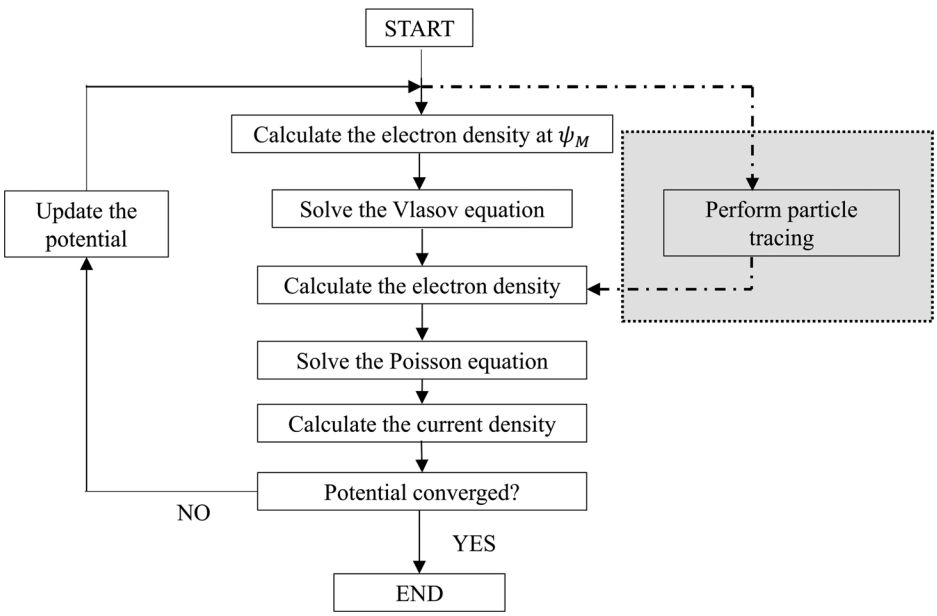

FIG. 2. Flowchart representation of the proposed self-consistent approach to calculate the output characteristics of TECs. Initially, the density of the electrons is assumed to be zero, and therefore only the Laplace equation is solved. In later iterations, the Poisson and Vlasov equations, or alternatively, Poisson and the particle tracing equations are self-consistently solved to reach convergence.

the collector and the emitter in the case that the workfunctions of the emitter and the collector are equal. In the more general case where the workfunctions are not equal, the electric potential difference between the points just outside the collector and the emitter is equal to $V-(\phi_E-\phi_C)/e$, where eV is the difference between the Fermi levels of the collector and the emitter (due to the applied voltage).

Equation (3) can be solved at each iteration by noting that $\psi(x)$ can be written as the sum of two functions, $\psi_l(x)+\psi_{dp}(x)$, where $\psi_l(x)$ represents the solution to the Laplace equation, $\frac{d^2\psi_l(x)}{dx^2}=0$, with $\psi_l(0)=0$ and $\psi_l(d)=eV$ boundary conditions; $\psi_{dp}(x)$ is the solution to the Poisson equation with the homogeneous Dirichlet boundary conditions, namely, Equation (3) subject to $\psi_{dp}(0)=\psi_{dp}(d)=0$, as the boundary conditions. In this 1-D example, $\psi_l(x)=\frac{x}{d}V$. $\psi_{dp}(x)$ is solved numerically by means of spatial discretization of the Laplacian operator

$$\frac{d^2}{dx^2}\approx\frac{1}{\Delta x^2}\begin{bmatrix}-2 & 1 & 0 & 0 & 0\\ 1 & -2 & 1 & 0 & 0\\ 0 & 1 & \ddots & \ddots & 0\\ 0 & 0 & \ddots & -2 & 1\\ 0 & 0 & 0 & 1 & -2\end{bmatrix} \tag{4}$$

and taking the inverse of the resulting sparse matrix. Δx represents the discretization distance. Since the sampling points remain the same within the entire calculations for a given set of variables, the inverse of the Laplacian matrix can be calculated only once to save on computation cost. (Meir *et al.*[5,15] arrived at an equivalent form of Equation (3) and used a non-linear solver to calculate the motive in the inter-electrode region.) An important numerical difficulty in solving Equation (3) can arise at higher values of γ_E at $x>x_M$ where the error function approaches 1. This issue can be bypassed by using an asymptotic expansion of the error function[23] and substituting the resulting function in Equation (3):

$$\begin{aligned}&\exp(\gamma_E)\left(1-\operatorname{erf}\left({\gamma_E}^{1/2}\right)\right)\\&=\frac{1}{\sqrt{\pi}}\left({\gamma_E}^{-1/2}-\frac{1}{2}{\gamma_E}^{-\frac{3}{2}}+\frac{3}{4}{\gamma_E}^{-\frac{5}{2}}-\cdots\right.\\&\left.+\frac{(-1)^{n+1}1\times3\times\cdots(2n-3){\gamma_E}^{n-1/2}}{2^{n-1}}+\cdots\right).\end{aligned} \tag{5}$$

Using the first 6 terms in Equation (5) leads to numerical errors less than 10^{-4} % for values of $\gamma_E>20$. After Poisson's equation is solved, the electric potential is updated as a mixture of the previous solution and the new solution to avoid large jumps in the potential, i.e., $\psi_{dp,n}(x)=(1-\alpha)\psi_{dp,n-1}(x)+\alpha\psi_{dp}(x)$, where α is the mixing ratio, and the subscript n represents the iteration number. This step is necessary due to the non-linearity of Equation (3), leading to a strong dependence of electron density on the potential profile. The mixing ratio needs to be chosen small enough so that large oscillations do not occur in smaller values of n, where the solutions of the Poisson and Vlasov equations are strongly decoupled. Values of $\alpha\le0.1$ were found to be suitable for the problems studied in this paper.

The current density can be equal to the maximum saturation current density, J_{sat}, determined by the Richardson-Dushman equation, if electrons do not face a potential barrier in the inter-electrode distance, i.e., when $x_M=0$. Therefore, $J=J_{sat}\exp(-\gamma_E(x=0))=J_{sat}\exp\left(-\frac{\psi_M}{k_BT_E}\right)$, which can be used to calculate the current at each iteration. The current density at each iteration is equal to the integral of the product of the x component of the velocity and the velocity distribution function

$$J=e\int_{-\infty}^{\infty}\int_{-\infty}^{\infty}\int_{-\infty}^{\infty}v_xf(x,v)\,dv_x\,dv_y\,dv_z=e\,n(x_M)\left(\frac{2\,k_B\,T_E}{\pi m}\right)^{1/2}. \tag{6}$$

The result in Equation (6) was calculated using Equation (1). This value of current density is expectedly independent of position. The electron density at the point of maximum motive, $n(x_M)$, can be derived from this result.

The new motive is subsequently incorporated into the Vlasov equation, and the loop is repeated until the motive converges. The convergence criterion is set such that the cumulative root mean square change in motive, $\sqrt{\frac{\sum\left(\psi_{dp}(x_i)-\psi_{dp,n-1}(x_i)\right)^2}{\sum\left(\psi_{dp,n-1}(x_i)\right)^2}}$, is less than 1 %.

Figure 3 presents the evolution of the motive as a function of the iteration number in the simulation. (The parameters of the TEC under study are $\phi_E=\phi_C=4.5$ eV, $T_E=2000$ K, and $d=10$ mm.) The convergence can usually be reached at iteration numbers less than 100. The entire simulation time on a regular modern PC is around 1–3 s when this model is implemented in MATLAB. The $n=1$

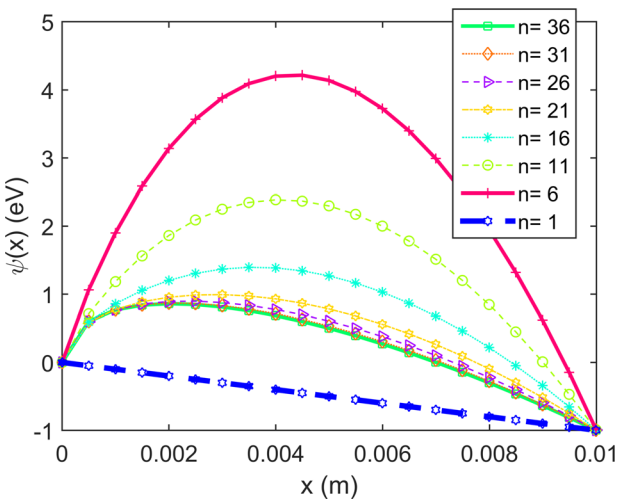

FIG. 3. The evolution of the motive vs. distance as the loop in Fig. 2 is repeated. n represents the iteration number. The $n=1$ case corresponds to the Laplace equation solution. This initial attempt underestimates the space-charge and therefore leads to high electron density. The exaggerated density results in higher space-charge effect ($n=6$), which in turn reduces the electron density in subsequent iterations. The parameters of the TEC under study are $\phi_E=\phi_C=4.5$ eV, $T_E=2000$ K, and $d=10$ mm.

case corresponds to the Laplace equation's solution. Initially, the space-charge motive is underestimated and therefore leads to high electron density. The exaggerated density causes higher motive due to space charge ($n = 6$), which in turn reduces the electron density in the subsequent iterations until convergence.

Particle tracing approach to bypass the analytical solution to the Vlasov equation

Here, we show that particle tracing can be used to bypass the analytical solution of the Vlasov equation. A finite difference time-domain (FDTD) particle-in-cell (PIC) approach to obtaining the output characteristics of thermionic convertors has been adopted by Lo *et al*. using a 1-dimensional object oriented particle tracing software package called OOPD1.[24] This method can be computationally expensive, since the electrons are followed in real time and their influence on each other is accounted for by solving the Poisson equation. Since we are interested in the steady state response of the system, we propose a particle tracing approach that can mimic the solving of the Vlasov equation and integration of the distribution function in an efficient manner. Instead of solving the Poisson equation at each time step as the electrons propagate, we solve the Poisson equation at the end of each iteration where the equilibrium electron density for that particular motive profile has been reached.

A flux of 10^7 electrons is released from the emitter at regular intervals, over a total duration of 5 μs (roughly 1000 times larger than the time-of-flight of the electron with an average velocity corresponding to 2000 K). The initial velocities of these electrons follow an HM distribution. The effective area of emission is adjusted so that the flux of the forward-moving electrons at the emitter matches the incident thermionic flux, J_{sat}/e. Using a higher number of incident electrons leads to a higher number of electrons in the inter-electrode region, although the overall electron density remains constant. These electrons are followed on their trajectory to the collector through the potential landscape produced in a previous step as the solution of the Poisson equation. The acting force at each particle position is calculated at a grid point and interpolated to the current position of the particle. The particle is propagated using a leapfrog algorithm:[25] $x_i = x_{i-1} + v_i\,\Delta t + \frac{1}{2}\frac{F(x_{i-1})}{m}\Delta t^2$ and $v_i = v_{i-1} + \frac{1}{2}\frac{\left(F(x_{i-1})+F(x_i)\right)}{m}\Delta t$, where x_i, v_i, and $F(x_i)$ are the position, velocity, and the acting force on the electron, respectively, at step i, and Δt is the time interval. Each electron "feels" the presence of the other electrons only though the Poisson equation in a mean field fashion. The electrons that are pushed back to the emitter or reach the collector are removed from the system, and their numbers are recorded (along with their arrival time) and used subsequently to calculate the current density. If the final position of an electron lies between two grid points, its charge is distributed between its nearest neighbors using a linear weighting function. The electron density obtained by coupling the particle tracing approach and the Poisson equation were compared with that of the Vlasov-Poisson system. The results are depicted in Fig. 4(a), when the solution has converged after 20 rounds of iteration. The fluctuations in the electron density are due to the element of randomness in the initial velocity of the electrons introduced by the random Gaussian distribution that was used to generate the initial velocities. However, these fluctuations are washed out in the double integration process of solving the Poisson equation, leading to the same motive and hence the same current (Fig. 4(b)). The number of the

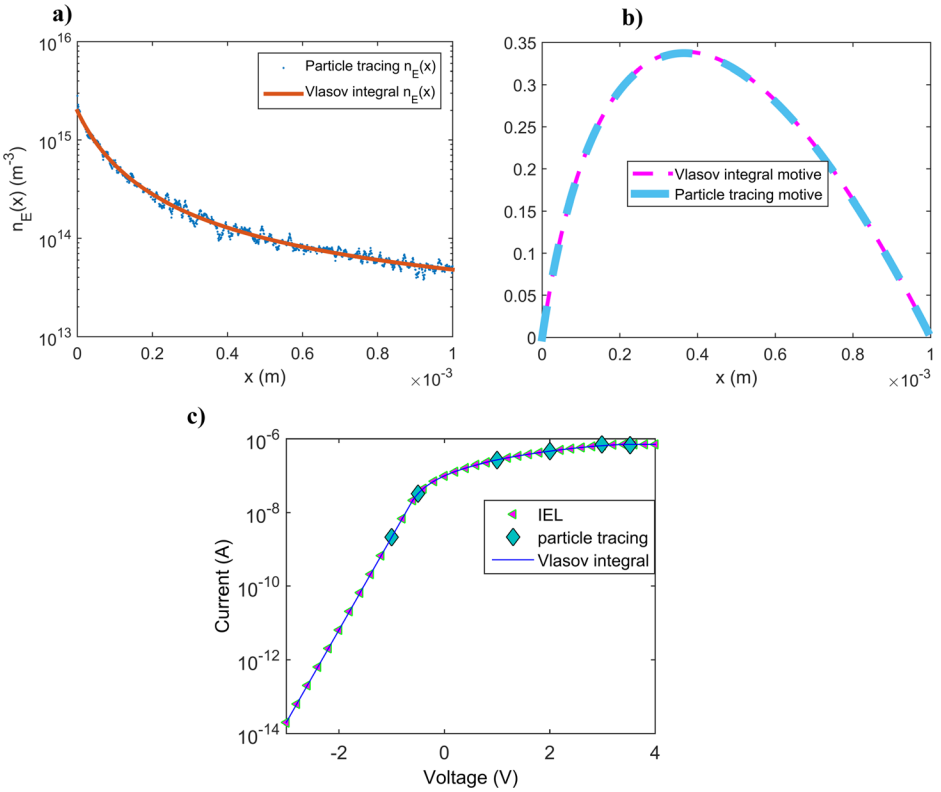

FIG. 4. Comparison between the particle tracing approach to calculate the electron density and the analytical Vlasov solution. The motive (a) and the electron density (b) for the final round of the iteration, when the convergence is reached, are plotted here. In the particle tracing approach, 10^7 particles are tracked in each iteration. This plot corresponds to the converged solution after 20 rounds of iteration. The electron density and motive plots from particle tracing are calculated based on their average steady-state values from 10 time steps. (c) Comparison between the improved-and-extended-Langmuir (IEL) and the numerical solutions (i.e., using Vlasov integrals or particle tracing) for the current-voltage characteristics of the same TEC as in part (a) with $\phi_E = 4.5$ eV, $T_E = 2000$ K, and $d = 1$ mm. (The overall current is calculated for an emission surface area of 3.14×10^{-8} m^2.) The IEL results were obtained based on the strategy outlined in Ref. 11. The particle tracing current is the average steady state value and matches the solutions obtained by applying an asymptotic expansion to the electron density.

emitted electrons should be chosen judiciously to ensure that the number of electrons in the inter-electrode region is higher than the number of grid points; otherwise, the resulting electron density becomes disjointed.

It is noted that this approach is more time-consuming (about 2–3 h on a regular PC) than using an analytical solution to the Vlasov equation (several seconds). However, the particle tracing approach is not limited to cases where an analytical solution to the Vlasov equation exists.

This model was applied to a wide range of the parameters of TECs, including different emitter temperatures, inter-electrode distances, and workfunctions. We used the analytical solutions that exist in this special case based on the IEL approach that we proposed in Ref. 11 to measure the numerical accuracy of this new self-consistent method. As depicted in Fig. 4(b), the results from this method are in complete agreement with those of the IEL approach. The parameters of the TEC under study are $\phi_E = \phi_C = 4.5\,\text{eV}$, $T_E = 2000\,\text{K}$, and $d = 1\,\text{mm}$. Furthermore, the solutions obtained by the asymptotic expansion of the electron density obtained from the Vlasov equation and the particle tracing approach completely agree with each other.

Self-consistent solution in the presence of back-emission

This model can be naturally extended to include the effect of electron emission from the collector as well. It is assumed that some electrons are emitted from the collector and are fully absorbed as they reach the emitter. The interaction between the electrons ejected from the emitter and collector in the inter-electrode region occurs through the Poisson equation; the motive is cast in the form $\psi(x) = \psi_l(x) + \psi_{dp,E}(x) + \psi_{dp,C}(x)$, where the last two terms represent the solutions to the Poisson equation with homogeneous Dirichlet boundary conditions for electron densities originating from the emitter and collector, respectively.

The ranges of velocities of the electrons originating from the collector can be worked out by using arguments similar to those in the previous section (Self-consistent solution in the absence of back-emission). Recalling that positive velocity is defined along the positive direction of the x axis, the maximum velocity is positive for electrons at $x \geq x_M$ and equal to $\left(2\frac{\psi_M-\psi(x)}{m}\right)^{\frac{1}{2}}$, which is the same as $v_{x,min}$ for electrons originating from the emitter; electrons originating from the collector can span the range from $-\infty$ to $v_{x,min}$. On the other hand, at $x < x_M$, the maximum velocity of the electrons originating from the collector is negative and equal to $-v_{x,min} = -\left(2\frac{\psi_M-\psi(x)}{m}\right)^{\frac{1}{2}}$. Therefore, the overall electron velocity distribution can be written as

$$f(x,v) = 2n_E(x_M)\left(\frac{m}{2\pi k_B T_E}\right)^{\frac{3}{2}} \exp\left(\frac{\psi_M-\psi(x)}{k_B T_E} - \frac{mv^2}{2k_B T_E}\right) \times \Theta(v_{ex} \mp v_{x,min}) + 2n_C(x_M)\left(\frac{m}{2\pi k_B T_C}\right)^{\frac{3}{2}} \times \exp\left(\frac{\psi_M-\psi(x)}{k_B T_C} - \frac{mv^2}{2k_B T_C}\right)\Theta(-(v_{ex} \mp v_{x,min})), \quad (7)$$

for $x \geq x_M$ (top sign) and $x < x_M$ (bottom). $n_E(x_M)$ and $n_C(x_M)$ represent the contributions of electrons arising from the emitter and the collector, respectively, to the electron density at the point of maximum motive.

Equation (7) is subsequently integrated to obtain the electron densities and replaced in the Poisson equation

$$\frac{d^2\psi(x)}{dx^2} = -\frac{e^2}{\epsilon_0} n(x_M) \begin{cases} \exp(\gamma_E)\left(1 - \text{erf}\left(\gamma_E{}^{1/2}\right)\right) + \exp(\gamma_C)\left(1 + \text{erf}\left(\gamma_C{}^{1/2}\right)\right), & x > x_M \\ \exp(\gamma_E)\left(1 + \text{erf}\left(\gamma_E{}^{1/2}\right)\right) + \exp(\gamma_C)\left(1 - \text{erf}\left(\gamma_C{}^{1/2}\right)\right), & x \leq x_M, \end{cases} \quad (8)$$

where $n(x_M) = n_E(x_M) + n_C(x_M)$ and $\gamma_C \equiv (\psi_M - \psi(x))/k_B T_C$. This equation is solved by the same strategy as in the last section (Self-consistent solution in the absence of back-emission). Additionally, by arguments similar to those preceding Equation (6), the overall current density at each iteration number is calculated as $J = J_{sat,E}\exp\left(-\frac{\psi_M}{k_B T_E}\right) - J_{sat,C}\exp\left(-\frac{\psi_M + eV}{k_B T_E}\right)$, where V is the potential difference between the points just outside the collector and emitter. The first term represents the contribution of the emitter to the total current density, J_E, whereas the second term is the contribution of the collector, J_C.

The value of $n(x_M)$ is calculated by individually equating J_E and J_C to the integral of the x component of the velocity and the velocity distribution functions, Equation (7), resulting in $J_E = e\,n_E(x_M)\left(\frac{2k_B T_E}{\pi m}\right)^{1/2}$ and $J_C = e\,n_C(x_M)\left(\frac{2k_B T_C}{\pi m}\right)^{1/2}$.

Until now, it was assumed that electrons maintain their temperatures as they propagate to the opposing electrodes. Since J_C and J_E depend on T_E and T_C, and the equation of continuity of charge dictates that $\nabla \cdot \boldsymbol{J}$ be constant in the steady-state, it follows that the electron temperature remains constant. The validity of this argument is nonetheless dependent on how well the velocity distribution of the electrons can be captured by an HM distribution at the point of the maximum motive. To calculate a limit on the validity of the HM distribution, the differential scattering cross-section formula[26] for the Coulomb

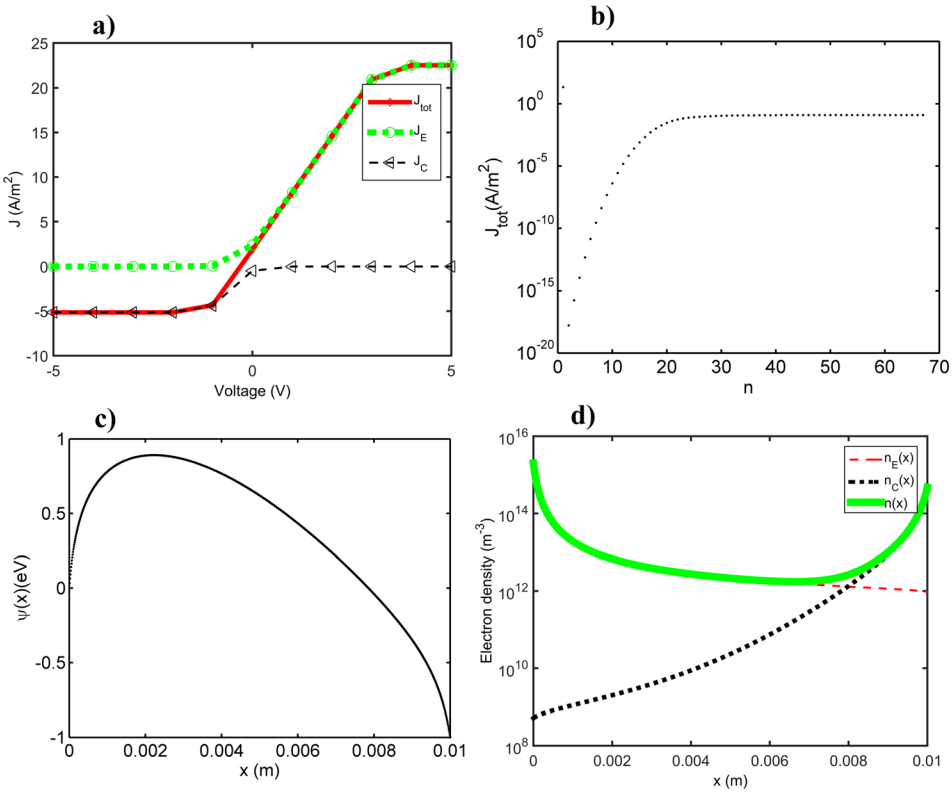

FIG. 5. (a) The contributions of the emitter and collector current densities, J_E and J_C, to the total current density, J_{tot}, of a TEC with $\phi_E = \phi_C = 4.5\,\text{eV}$, $T_E = 2000\,\text{K}$, $T_C = 1900\,\text{K}$, and $d = 1\,\text{cm}$. (b) The evolution of the total current density as a function of the iteration number, n. (c) The converged motive as a function of position for an applied voltage of 1 V. (d) The contributions of the electrons originating from the emitter and the collector to the overall electron density as a function of position.

interaction potential between two electrons was considered. The total scattering cross-section, σ_{tot}, can be calculated by integrating the differential scattering cross-section, resulting in infinity. However, the HM approximation becomes invalid when the scattering angle is more than 90°. Using this angle as the lower bound leads to the following non-HM total scattering cross-section: $\sigma_{tot,nHM} = \pi\left(\frac{e^2}{2\pi\epsilon_0 m v_{rel}^2}\right)^2$, where v_{rel} is the relative velocity between the electrons. The distance that electrons travel before this effect is considerable can be approximated as $(n(x)\,\sigma_{tot,nHM})^{-1}$. In the case of the device examples analyzed in this article, this distance is $\sim 700\,\text{m}$. Even for a high-performance TEC with $\phi_E = 2.0\,\text{eV}$ and $T_E = 1600\,\text{K}$, this distance is $\sim 200\,\mu\text{m}$. Given that a modern TEC can easily have an inter-electrode distance smaller than this, our model has a very broad range of applicability.

The contributions of the emitter and collector current densities, J_E and J_C, to the total current density, J_{tot}, of a TEC with $\phi_E = \phi_C = 4.5\,\text{eV}$, $T_E = 2000\,\text{K}$, $T_C = 1900\,\text{K}$, and $d = 1\,\text{cm}$ are presented in Fig. 5(a). The evolution of the total current density as a function of the iteration number, n, is plotted in Fig. 5(b). In the case of an applied voltage of $1\,V$, the converged motive as a function of position is displayed in Fig. 5(c). Finally, the contributions of the electrons arising from the emitter and the collector to the overall electron density are depicted in Fig. 5(d). Expectedly, the electron density arising from the emitter has its maximum around the emitter, whereas the electrons originating from collector are mostly concentrated in the proximity of the collector. Therefore, the overall electron density has two maxima in the presence of back-emission.

Lastly, it is noted that the methods developed in this paper can be used to calculate the output characteristics of TECs for a wide range of workfunctions, temperatures, applied voltages, and inter-electrode distances. This model applies as long as the quantum effects (e.g., tunneling in nanoscale gaps) and relativistic effects (at extremely high biases and not applicable in the power generation mode) are negligible. The cases studied here were deliberately chosen to have high space-charge (and naturally small output power density) so that electron transport in these conditions could be investigated. The maximum output power density as a function of inter-electrode gap size is shown in Fig. 6. It is

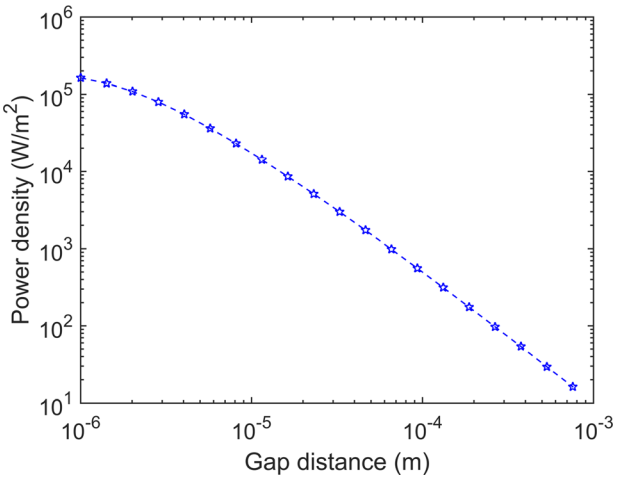

FIG. 6. The maximum output power density of a TEC as a function of the inter-electrode distance. The device parameters are $\phi_E = 2.5\,\text{eV}$, $\phi_C = 2.0\,\text{eV}$, $T_E = 1800\,\text{K}$, and $T_C = 700\,\text{K}$. The proposed method was employed to calculate the output current density at different voltages. These values were subsequently used to calculate the power density. The maximum power density was found by sweeping the voltage and calculating the current at each value of the gap size, due to the space-charge effect.

assumed that $\phi_E = 2.5\,\text{eV}$, $\phi_C = 2.0\,\text{eV}$, $T_E = 1800\,\text{K}$, and $T_C = 700\,\text{K}$. Based on the proposed method, for each gap size, the output current density for various applied voltages was calculated and subsequently used to calculate the power density. The maximum value of power density at each gap size (which occurs at different voltages for different gaps) was used to produce the data in Fig. 6. Expectedly, at smaller gaps where the space-charge effects are less palpable, the change in the maximum power density as a function of distance is slower than at the higher distances, where the space-charge effects are more prominent. These trends are in accordance with the power densities calculated in other works.[8]

SUMMARY

We presented a self-consistent approach to derive the characteristics of thermionic energy convertors. In the case that the analytical solution of the Vlasov equation is not possible, our model uses a particle tracing approach to calculate the electron densities. Moreover, by introducing an asymptotic expansion to deal with the ill-behaving functions, the range of applicability of our approach is significantly increased in the presence of an analytical solution. The model also circumvents the splicing issues and captures the entire characteristics of thermionic convertors. The results of this strategy were shown to be in agreement with previous solutions in the absence of back-emission. Subsequently, this method was employed to calculate the output characteristics of thermionic convertors in the presence of back-emission.

ACKNOWLEDGMENTS

We thank George A. Sawatzky for fruitful discussions. Financial support was provided by the Natural Sciences and Engineering Research Council of Canada (SPG-P 478867) and the Peter Wall Institute for Advanced Studies. Amir H. Khoshaman also thanks the University of British Columbia for additional support.

APPENDIX: CONVERGENCE OF THE SOLUTIONS TO THE POISSON-VLASOV SYSTEM

As with any two coupled differential equations with necessarily shared parameters, one expects that three scenarios could arise: the solutions to the two equations diverge, oscillate, or converge in each subsequent step. Divergence, in an absolutely mathematical sense, could occur if the two equations are incompatible with each other, i.e., the increments at each step amplify each other because a common solution to the two equations does not exist. Another type of diverging solution can arise even for compatible equations when the damping ratio is not chosen properly, and the intermediary solutions exceed the maximum finite floating-point number permissible in the programming language. The other possibility is for the solutions to oscillate, which could occur in cases where a common solution to the two equations does not exist, although the changes do not amplify each other (i.e., the electron density is not an increasing function of motive, whereas the motive is an increasing function of electron density), or if a small value of a damping ratio is chosen. Lastly, the equations can converge if they share a common solution and if a proper damping ratio is selected. The diverging solutions should be ruled out in the Poisson-Vlasov system, since the changes in one do not amplify the solutions of the other; e.g., incrementing the motive would significantly reduce the number of electrons with enough kinetic energy to overcome the maximum barrier, leading to reduced potential in the next step. Therefore, it remains to investigate if the Poisson-Vlasov system belongs to the oscillating type or the converging type.

It can be seen that the steady state response of a TEC in the absence of ions or alternating potentials (all the cases studied in this paper) belongs to the converging category by performing the following analysis:

1. Choose a value of $0 < \alpha < 0.1$ and run the simulation.
2. If the solution converged after a certain iteration number, n, set α to a higher value, i.e., 0.2 and run the simulation again to a high number of iterations (e.g., $n = 1000$). If the solution starts to oscillate, it shows that the system does not have a common solution to both equations. However, if the solution remains constant in the succeeding iterations, the system has settled on the common solution between the two equations. The latter occurs in all cases that we have studied. The mixing ratio, α, cannot be set to its maximum, i.e., 1. This is because the solution to the Poisson equation is calculated numerically, and its accuracy is determined by the fineness of the mesh. The slightest numerical mismatch in the motive (an error on the order of 10^{-10}) can grow exponentially due to the highly nonlinear nature of the Vlasov equation. For our cases, the number of mesh elements in the inter-electrode region is 1000. A mixing ratio of 0.2 was found to be enough to dampen the numerical errors that arise from the finite size of the mesh elements plus all the numerical errors in the other calculations.
3. If the solution oscillates and never reaches convergence, use a smaller value of α, but continue the simulation to a higher number of iterations, since the changes at each step have been damped more severely.
4. Go back to 2 (if the solution converged) and 3 (if the solution was oscillatory).

If the solution is always oscillatory (step 3), it can be imagined that a common solution to the two equations does not exist. This has never been observed for the cases that we have studied. A complete proof of the oscillatory nature of the solution would require an infinite number of iterations, with ever smaller values of α. This is obviously not feasible using a computer, since the smallest floating-point number of the programming language would soon be reached. However, this has never been observed in our cases (depending on the value of α, the test ends immediately in step 2 with non-oscillatory solutions, or for higher values of α in step 3 for one iteration and subsequently in step 2 with a non-oscillatory solution.) Therefore, this could be considered an *a posteriori* proof for the convergence of the solutions of the Poisson-Vlasov system in the steady state response of the TECs in the absence of ions or alternating currents.

An *a priori* argument for the existence of converging solutions to the Poisson-Vlasov system in the space-charge limited regime can be deduced from the work of Langmuir and Hatsopoulos,[9,10] where they present a closed-form solution to the system, signifying a unique current associated with each voltage in the space-charge limited mode, in the absence of the back-emission. In the saturation regime, the current is constant (for as long as the Schottky effect is negligible). In the retarding mode, there is also a unique correspondence between the current and the applied voltage.

[1]T. L. Westover, A. D. Franklin, B. A. Cola, T. S. Fisher, and R. G. Reifenberger, J. Vac. Sci. Technol., B **28**, 423 (2010).
[2]V. Robinson, T. Fisher, J. Michel, and C. Lukehart, "Work function reduction of graphitic nanofibers by potassium intercalation" (Birck NCN Publications, 2005).
[3]A. H. Khoshaman, H. D. E. Fan, A. T. Koch, N. H. Leung, and A. Nojeh, in *Proceedings of the 27th of the International Vacuum Nanoelectronics Conference (IVNC)* (2014), pp. 59–60.
[4]J. R. Smith, G. L. Bilbro, and R. J. Nemanich, J. Vac. Sci. Technol., B **27**, 1132 (2009).
[5]S. Meir, C. Stephanos, T. H. Geballe, and J. Mannhart, J. Renewable Sustainable Energy **5**, 043127 (2013).
[6]J. H. Lee, I. Bargatin, T. O. Gwinn, M. Vincent, K. A. Littau, R. Maboudian, Z.-X. Shen, N. A. Melosh, and R. T. Howe, in *Proceedings of the IEEE 25th International Conference on Micro Electro Mechanical Systems (MEMS)* (2012), pp. 1261–1264.
[7]A. Khoshaman, H. D. E. Fan, A. Koch, G. Sawatzky, and A. Nojeh, IEEE Nanotechnol. Mag. **8**, 4 (2014).
[8]G. N. Hatsopoulos and E. P. Gyftopoulos, *Thermionic Energy Conversion* (The MIT Press, 1973), Vol. 1.
[9]I. Langmuir, Phys. Rev. **21**, 419 (1923).
[10]G. N. Hatsopoulos and E. P. Gyftopoulos, *Thermionic Energy Conversion–Vol. 2: Theory, Technology, and Application* (The MIT Press, 1979).
[11]A. H. Khoshaman, A. T. Koch, M. Chang, H. D. E. Fan, M. V. Moghaddam, and A. Nojeh, IEEE Trans. Nanotechnol. **14**, 624 (2015).
[12]A. H. Khoshaman, M. Chang, H. D. E. Fan, A. T. Koch, and A. Nojeh, in *Proceedings of the IEEE 14th International Conference on Nanotechnology (IEEE-NANO)* (2014), pp. 682–684.
[13]A. H. Khoshaman, M. Chang, and A. Nojeh, in *Proceedings of the 26th International Vacuum Nanoelectronics Conference (IVNC)* (2013), pp. 1–2.
[14]J. R. Smith, G. L. Bilbro, and R. J. Nemanich, Phys. Rev. B **76**, 245327 (2007).
[15]S. Meir, Highly-efficient conversion of heat and solar radiation into electricity. Ph.D. thesis (Universität Augsburg, 2012).
[16]J. R. Smith, J. Appl. Phys. **114**, 164514 (2013).
[17]J.-H. Lee, I. Bargatin, N. A. Melosh, and R. T. Howe, Appl. Phys. Lett. **100**, 173904 (2012).
[18]C. Stephanos, *Thermoelectronic Power Generation from Solar Radiation and Heat* (Universität Augsburg, 2012).
[19]A. F. Dugan, J. Appl. Phys. **31**, 1397 (1960).
[20]C. R. Crowell, Solid-State Electron. **8**, 395 (1965).
[21]F. F. Chen, *Introduction to Plasma Physics and Controlled Fusion. Volume 1, Plasma Physics*, 2nd ed. (Springer, New York, 2006).
[22]J. A. Bittencourt, *Fundamentals of Plasma Physics* (Springer, New York, 2004).
[23]G. B. Arfken and H. J. Weber, *Mathematical Methods for Physicists, Seventh Edition: A Comprehensive Guide*, 7th ed. (Academic Press, Amsterdam; Boston, 2012).
[24]F. S. Lo, P. S. Lu, B. Ragan-Kelley, A. J. Minnich, T. H. Lee, M. C. Lin, and J. P. Verboncoeur, Phys. Plasmas **21**, 023510 (2014).
[25]C. K. Birdsall and A. B. Langdon, *Plasma Physics via Computer Simulation*, 1st ed. (CRC Press, 2004).
[26]L. D. Landau and L. D. Landau, *Mechanics* (Pergamon, Oxford, 1960).